Modeling and Design of an Integrated Winding Synchronous Permanent Magnet Planar Motor

Lu Zhang, Baoquan Kou, Liyi Li and Binchao Zhao

Department of Electrical Engineering, Harbin Institute of Technology, Harbin, 150001 China

***Abstract*—This paper presents a novel integrated winding synchronous permanent magnet planar motor(IWSPMPM), which is driven by composite currents. In this research, the flux density distribution of a two-dimensional magnet array used for the IWSPMPM was obtained by solving the scalar magnetic potential. Expressions of the electromagnetic forces and back-EMF of the IWSPMPM were derived. Based on this, the main dimension of the IWSPMPM was confirmed, also the expression was derived. The design of the coil and permanent magnet was studied respectively, effects of the height of the coil and the thickness of the magnet on the electrical properties of the planar motor were analyzed. A prototype motor is manufactured, and some experiments were carried out with it. Both measurement and simulation coincide well.**

***Index Terms*—planar motor, analytical model, electrical property**

I. Introduction

Direct drive of multi degrees of freedom is one of the key technologies for higher motor-drive performance and more precise positioning in various industrial fields. As a result, the planar motors, which can move freely on a flat, have received increasing attention. Currently, many types of planar motors have been proposed. According to the operation principle, they can be classified into variable reluctance planar motors [1], [2], induction planar motors [3], [4], synchronous permanent magnet planar motors(SPMPM) [5]-[11], DC planar motors [12-14] and some other planar motors with special structures, such as ultrasonic planar motor [15], [16]. Among them, the SPMPM has many advantages such as direct driving, low friction, no backlash, high accuracy, and can be used in extreme-UV lithography equipment.

In this paper, we propose a novel integrated winding synchronous permanent magnet planar motor(IWSPMPM), as shown in Fig. 1. Compared with the planar motor proposed in [5]-[8], [17], composite-current driven synchronous permanent magnet planar motor proposed in this paper have many advantages. Firstly, utilization of the armature windings is increased, quality of the mover is reduced correspondingly, and the dynamic performance is improved too. Secondly, a wide range of movement can be achieved easily since structure of the permanent magnet array is simple. In addition, there is no cogging force due to the coreless structure.

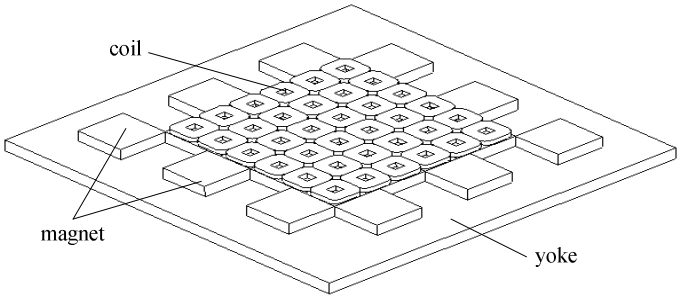

Fig. 1. Scheme of the IWSPMPM.

II. Analytical Model

A. Magnetic Field of the Magnet Array

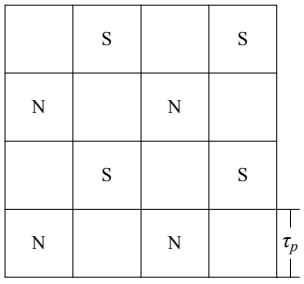

Fig. 2. Permanent magnet array.

Fig. 2 shows the permanent magnet array used in this paper which was proposed by Asakawa in 1986's patent[18]. Here, N means the direction of the magnetic field going out from the paper, and S means going to the paper, the other blanks denote air. As finite element method time consuming, analytical method will be adopted to obtain the magnetic field, and before analysis some assumptions will be made in order to simplify the model[19-21]. The relative permeability of the iron yoke has a value of infinity, the motor has a periodicity over the x and y direction and the magnetization value of the permanent magnet is not changed.

By solving the equations of the scalar magnetic potential, the z-component of air-gap flux density distribution can be expressed as following

978-1-4673-0305-7/12/$31.00 ©2012.IEEE

$$B_{gz}(x,y,z)=\frac{2B_r}{k\pi}\left[\sin(a_k x)+\sin(a_k y)\right]\times\frac{\sinh(a_k h_m)\cosh\left[a_k(z-4h_m)\right]}{sch_k} \quad (1)$$

where h_m is the thickness of permanent magnet magnetization, $a_k=k\pi/\tau_p$, $sch_k=\mu_r\sinh(3a_kh_m)\cosh(a_kh_m)+\cosh(3a_kh_m)\sinh(a_kh_m)$.

For simplicity, the flux density distribution in the air gap is assumed to be a two dimensional sinusoidal wave, and when calculating electromagnetic thrust only fundamental will be considered. Therefore, the expression of the z-directional air-gap flux density will be expressed as

$$B_{gz}(x,y)=B_{mz}\left[\sin(a_1x)+\sin(a_1y)\right] \quad (2)$$

where

$$B_{mz}=\frac{1}{h_c}\int_{h_m+g}^{h_m+g+h_c}\frac{2B_r\sinh(a_1h_m)\cosh\left[a_1(z-4h_m)\right]}{\pi sch_1}dz$$

B. Thrust and Back-EMF

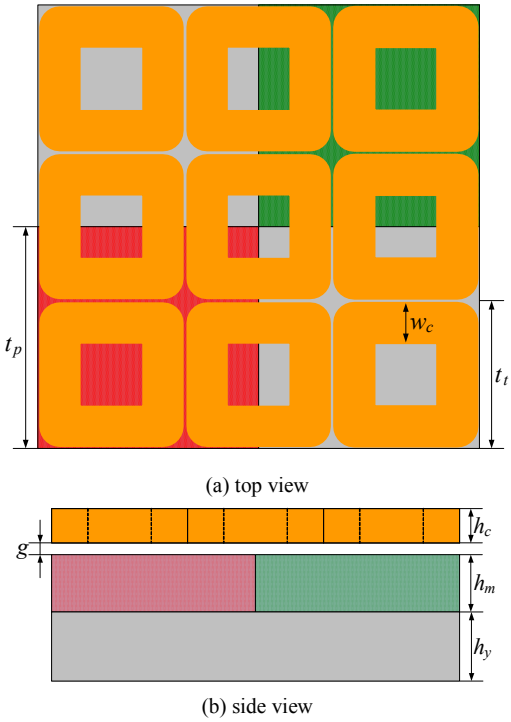

Fig. 3. The unit planar motor

Fig. 3 shows the scheme of the unit planar motor. As the stationary permanent magnet arrays adopt the configuration of the same shape viewed from the x and y side, so the thrust of the coils in the x- and y- directions are the same. Based on the Lorentz law, thrust of the unit planar motor can be expressed as

$$F=3\sqrt{2}N\cdot B_{mz}\cdot I\cdot(2\tau_p-3w_c)\sin\left(\frac{\pi}{3}-\frac{\pi w_c}{2\tau_p}\right) \quad (3)$$

where N is the turns of a coil, w_c is the width of a coil.

The thrust density ρ_F is defined as

$$\rho_F=\frac{F}{V} \quad (4)$$

where $V=2\tau_p\times2\tau_p\times(h_y+h_m+h_c+g)$ is the effective volume(the volume of the coupling part of the mover and stator), h_y is the thickness of yoke, h_c is the thickness of coil and g is the length of air-gap.

In Fig.3, assuming the coils moves in the x-direction with a constant velocity v, the expression of the back-EMF of coils with N turns is

$$E=\sqrt{2}N\cdot B_{mz}\cdot v\cdot(2\tau_p-3w_c)\sin\left(\frac{\pi}{3}-\frac{\pi w_c}{2\tau_p}\right) \quad (5)$$

III. Design of the Planar Motor

A. Major Dimension

The key of design a motor is to determine the main dimensions of the motor. In this paper, the pole pitch τ_p is the main dimension of the planar motor. Ignoring mechanical losses and iron losses , the electromagnetic power can be expressed as following

$$mEI\cos\psi=F_N v \quad (6)$$

where m is the phase number, E is the EMF, I is the phase current, F_N is the rated thrust, v is the velocity, ψ is the angle between E and I.

According to the structure of the planar motor, the line load is defined as

$$A=\frac{2mNI}{2\tau_p}=\frac{mNI}{\tau_p} \quad (7)$$

By substituting (3) and (7) into (6), the main dimensions' equation can be derived as following

$$\frac{\tau_p(2\tau_p-3w_c)\sin(\frac{\pi}{3}-\frac{\pi w_c}{2\tau_p})}{F_N}=\frac{\sqrt{2}/2}{AB_{mz}} \quad (8)$$

B. Influence of dimensions of coils

The hight and width of the coil are important parameters of the planar motor because they affect the motor performance, such as the thrust, the thrust density, and the thrust ripple. When the turns N and wire diameter d_c is determined, cross-sectional area of the winding will be fixed. As the magnetic field generated by permanent magnet arrays is a three-dimensional field in the space, the flux density decreases exponentially in the vertical direction and has sinusoidal periodic in the horizontal direction. So, thrust generated by the unit planar motor will vary with the different h_c and w_c.

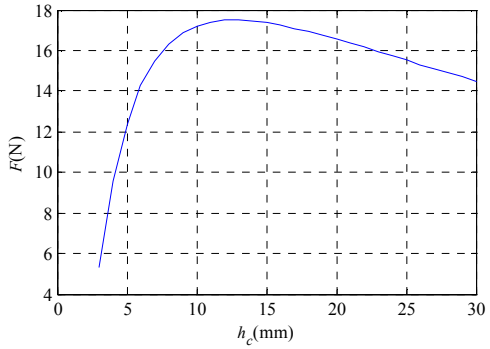

Fig. 4. Thrust F generated by unit planar motor varied with hc.

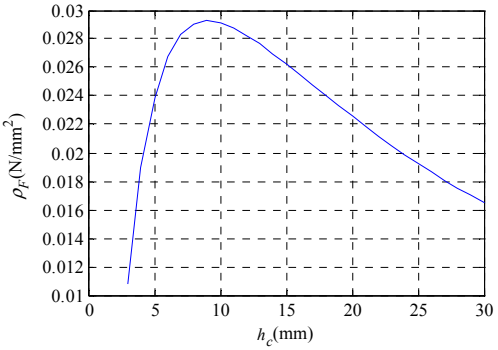

Fig. 5. Thrust density ρF varied with hc.

Fig. 4 shows the electromagnetic thrust generated by a unit planar motor vary with the height of the coil. With the h_c increasing, the electromagnetic thrust first increases and then decreases. And there is a certain h_c that makes the electromagnetic thrust getting its maximum value.

Fig. 5 shows the electromagnetic thrust density of the unit planar motor vary with the height of the coil. It can be seen that with the increase of the h_c, the thrust density increases fast and then decreases slowly. Also, there is a certain h_c that makes the electromagnetic thrust density getting its maximum value.

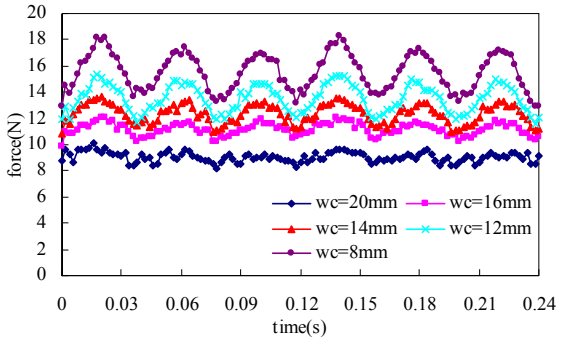

Fig. 6. Forces of the unit planar motor with different w_c.

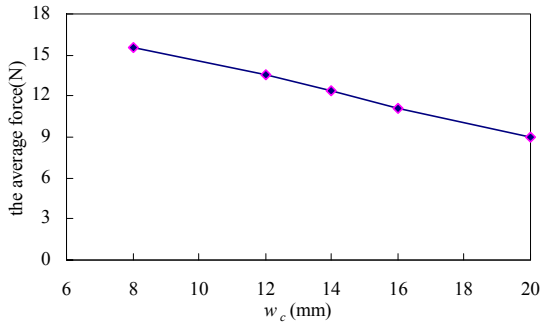

Fig. 7. The average thrust of the unit planar motor vary w_c.

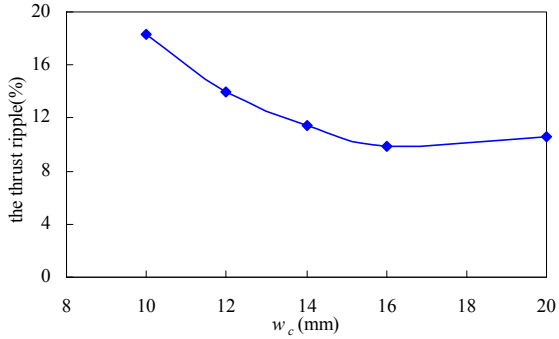

Fig. 8. The thrust ripple of the unit planar motor vary w_c.

Fig. 6 shows force of the unit planar motor with different w_c. Fig. 7 and Fig. 8 show the average thrust and the thrust ripple of the uint planar motor vary w_c respectively. When w_c=20mm, the electromagnetic thrust of the unit planar motor is small, as the effective length of inner layer coil is short. But at this time, it has a smaller thrust ripple as high harmonic has little effect on magnetic field. With the w_c decreases , the effective length of inner layer coil and the effects of the higher harmonic increase, so the electromagnetic thrust increases, and the thrust ripple become bigger.

C. Influence of hight of permanent magnet

For permanent magnet, the magnetization thickness is an important parameters of the planar motor because it affects the motor performance, such as the magnetic field and the thrust of the planar motor.

The magnetic field produced by the permanent magnet array has been obtained analytically by solving the equations using the scalar magnetic potential. In magnetic field, the ratio of the fundamental can be defined as following

$$\delta_1 = \frac{M_1}{\sqrt{M_1^2 + M_3^2 + M_5^2 + \cdots M_{2n+1}^2}} \tag{9}$$

where M_1 is the amplitude of the fundamental, M_{2n+1} is the odd harmonics' amplitude, n=1,2…

Fig. 9 shows the amplitude of the B_{gz1} vary with the magnetization thickness. The graph shows the amplitude of the

fundamental is very small when the magnetization thickness is small. With the magnetization thickness increases, the amplitude increase quickly. However, after the magnetization thickness comes to 50mm, the amplitude almost has no changing.

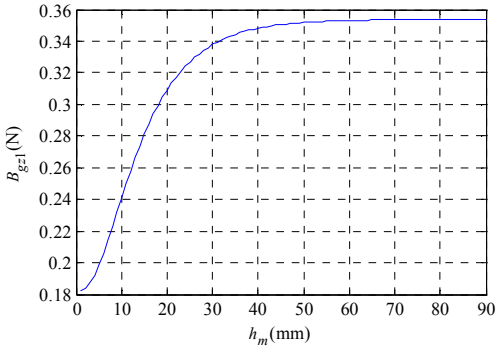

Fig. 9. Peak value of B_{g1} versus h_m.

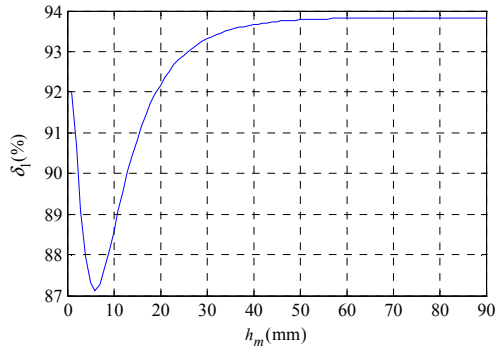

Fig. 10. The ratio of the fundamental versus h_m.

Fig. 10 shows the ratio of the fundamental vary with the magnetization thickness of the permanent magnet. It can be observed that the ratio of the fundamental is large when the magnetization thickness is small. However, at this point the amplitude of the fundamental is too small as shown in Fig. 9. With the increase of the magnetization thickness, the ratio of the fundamental comes to the minimum. Then the ratio of the fundamental increases quickly with the continuing incrassation. Similarly, the ratio of the fundamental increases little when the magnetization thickness comes to a certain degree.

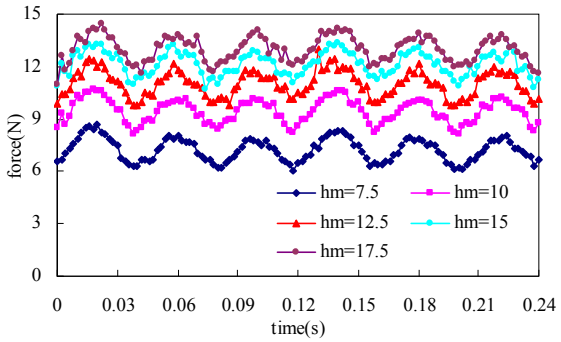

Fig. 11. Forces of the unit planar motor with different h_m.

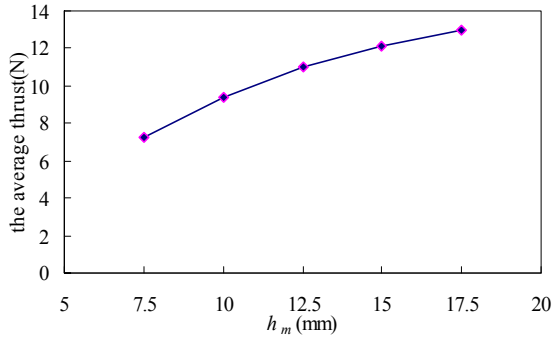

Fig. 12. The average thrust of the unit planar motor vary h_m.

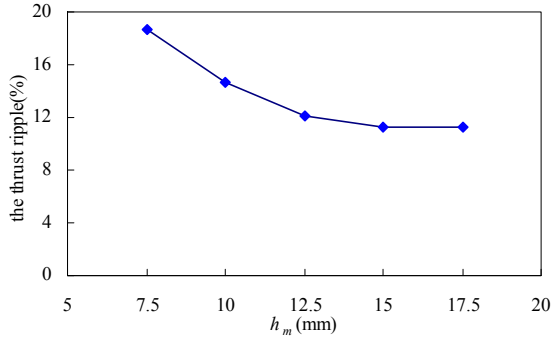

Fig. 13. The thrust ripple of the unit planar motor vary h_m.

Fig. 11 shows thrust-time curves for different magnetization thickness of the unit planar motor. Fig. 12 and Fig. 13 show the average thrust and the thrust ripple of the unit planar motor varying with the magnetization thickness respectively. As shown in Fig. 12 and Fig. 13, due to the great effects that the magnetization thickness affect on the air-gap magnetic field, when the magnetization thickness increases, the average thrust of the planar motor increases too. With the increasing of the magnetization thickness, the influence of the harmonic becomes smaller, so the thrust ripple becomes smaller also. In Fig. 13, it can be observed that the thrust ripple nearly has no changes after the magnetization thickness reaches 15 mm.

IV. Prototype and Experiment

A. Prototype

Based on the previous analysis in this paper, a prototype of the IWSPMPM has been designed and manufactured, as shown in Fig. 14. Table I shows the specification data of the IWSPMPM. And some experiments were carried out with the prototype.

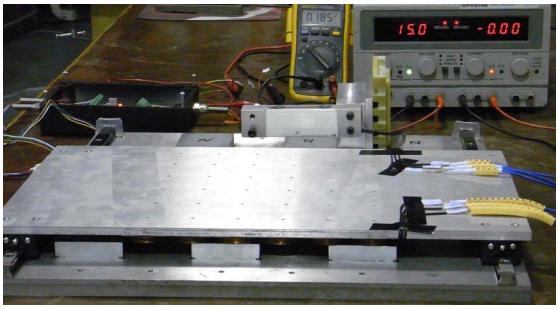

Fig. 14. The prototype.

TABLE I
DIMENSIONS OF THE MANUFACTURED MOTOR

Part	Item	Symbol	Value	Unit
Mover	pitch of the coil	τ_t	40	mm
	coil cross-section width	w_c	14	mm
	coil cross-section height	h_c	5.7	mm
	winding turns	N	125	
	wire diameter	d	0.76	mm
Air-gap	length	g	1	mm
Stator	pitch of the magnet	τ_p	60	mm
	thickness	h_m	15	mm

B. *The results comparison*

To verify the linearity of the static thrust, the input current of one phase was changed and the static thrust was measured. Fig. 15 shows the curves of maximum static thrust versus input current. It can be found that the trend of the curves is basically linear. Fig. 16 shows the peak value of B_g versus the distance from magnet surface. We can see that the flux density decreases exponentially with the air-gap length. The EMF in one phase winding is measured, while the mover is moved in the x-direction at constant speed(v_x=0.5m/s). Fig. 17 shows the result. From Fig. 15, Fig. 16 and Fig. 17, it can be observed that both of the measurement and simulation coinside well

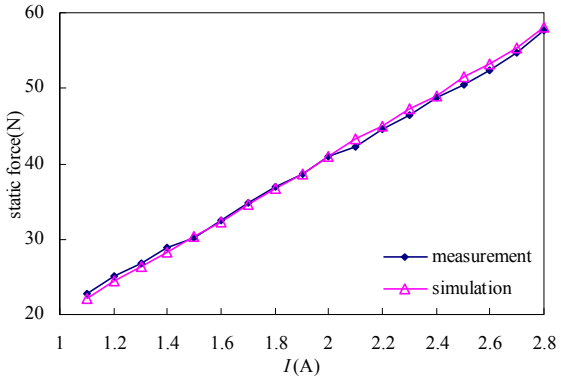

Fig. 15. The curve of the static force according to input current.

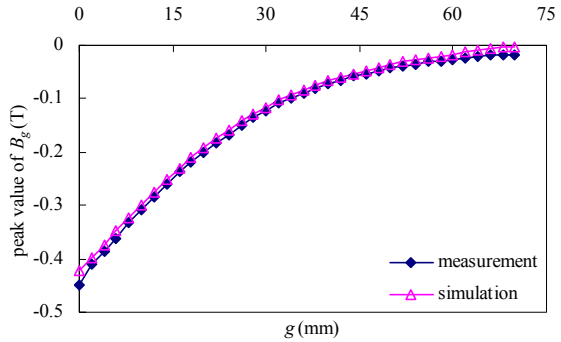

Fig. 16. Peak value of Bg versus distance from magnet surface.

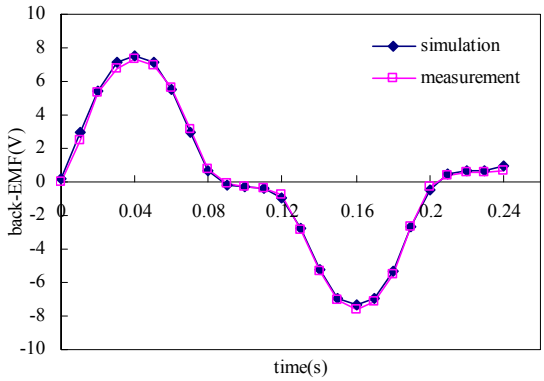

Fig. 17. The back-EMF waveform of the planar motor.

V. CONCLUSIONS

In this paper, we proposed a novel composite-current driven integrated winding synchronous permanent magnet planar motor. Flux density of the magnet array was solved analytically by solving the scalar magnetic potential equations. The expression of air-gap flux density in the z-direction has been acquired. Some important parameters of the planar motor have been analyzed, and a prototype of the IWSPMPM has been manufactured. The magnetic field, static thrust and back-EMF experiments were performed to validate the simulation results.

Compared with conventional synchronous permanent magnet planar motors, the novel IWSPMPM proposed in this paper has high utilization of armature windings, good dynamic performance and no cogging force. Hence it is allowed to apply this planar motor to ultra-precise two-dimensional plane driven devices.

ACKNOWLEDGMENT

The work described in this paper was supported by the National S&T Major Project (2009ZX02207-001) and Program for New Century Excellent Talents in University (NCET-08-0158).

REFERENCES

[1] J. F. Pan, N. C. Cheung, W. C. Gan, "A novel planar switched reluctance motor for industrial applications," *IEEE Trans. Magn.*, vol. 42, no. 10, pp. 2836-2839, Oct. 2006.

[2] J. I. Shalom, "Modeling of sawyer planar sensor and motor dependence on planar yaw angle rotation," *IEEE Intel. Conf. Robotics and Automation Albuquerque*, New Mexico, pp. 3499-3504, Apr. 1997.

[3] N. Fujii, and M. Fujitake, "Two-dimensional drive characteristics by circular shaped motor," *IEEE Trans. Ind. Applicat.*, vol. 35, no. 4, pp. 803-809, Jul./Aug. 1999.

[4] Peter Dittrich, "3-DOF planar induction motor," *IEEE Intel. Conf. Electro/information Technology*, pp. 81-86, May. 2006.

[5] H. S. Cho, and H. K. Jung, "Analysis and design of synchronous permanent-magnet planar motors," *IEEE Trans. Energy Conversion*, vol. 17, no. 4, pp. 492-499, Dec. 2002.

[6] Jiayong Cao, Yu Zhu, Jinsong Wang, "A novel synchronous permanent magnet planar motor and its model for control applications," *IEEE Trans. Magn.*, vol. 41, no. 6, pp. 2156-2162, Jun. 2005.

[7] J. W. Jansen, C. M. M. van Lierop, E. A. Lomonova, and A. J. A. Vandenput, "Modeling of magnetically levitated planar actuators with moving magnets," *IEEE Trans. Magn.*, vol. 43, no. 1, pp. 15-25, Jan. 2007.

[8] J. de Boeij, E. Lomonova, and A. J. A. Vandenput, "Optimization of contactless planar actuator with manipulator," *IEEE Trans. Magn.*, vol. 44, no. 6, pp. 1118-1121, Jun. 2008.

[9] J. W. Jansen, C. M. M. van Lierop, E. A. Lomonova, and A. J. A. Vandenput, "Magnetically levitated planar actuator with moving magnets," *IEEE Trans. Ind. Applicat.*, vol. 44, no. 4, pp. 1108-1115, Jul./Aug. 2008.

[10] J. de Boeij, E. Lomonova, and J. Duarte, "Contactless planar actuator with manipulator: a motion system without cables and physical contact between the mover and the fixed world," *IEEE Trans. Ind. Applicat.*, vol. 45, no. 6, pp. 1930-1938, Nov./Dec. 2009.

[11] Y. Ueda and H. Ohsaki, "A planar actuator with a small mover traveling over large Yaw and translational displacements," *IEEE Trans. Magn.*, vol. 44, no. 5, pp. 609-616, May.2008.

[12] W. Gao, S. Dejima, H. Yanai, "A surface motor-driven planar motion stage integrated with an *x-y-θ-z* surface encoder for precision positioning," *Precision Eng.*, no. 28, pp. 329-337, 2004.

[13] A. F. Flores, A. A. Susin, and M. A. da Silveira, "Application of Neodymium-Iron-Boron permanent magnets on the assembling of a novel planar actuator," *IEEE Trans. Magn.*, vol. 35, no. 5, pp. 4034-4036, Sep.1999.

[14] Baoquan Kou, He Zhang, Liyi Li, "Analysis and Design of a Novel 3-DOF Lorentz-Force-Driven DC Planar Motor," *IEEE Trans. Magn.*, vol. 47, no. 8, pp. 2118-2126, Aug.2011.

[15] C. D. Li, S. Xu, R. F. Liu, "Dynamic analysis and optimal design of a novel small 2-D planar ultrasonic motor," *IEEE Ultrasonic Motor*, pp. 2269-2272, 2006.

[16] S. J. Shi, J. K. Liu, W. S. Chen, Y. X. Liu, "Development of a 2-DOF planar ultrasonic motor using longitudinal-bending hybrid transducer," *IEEE International Symposium on the Applications of Ferroelectrics*, pp. 1-5, 2009.

[17] W. J. Kim, "High-precision planar magnetic levitation," Ph.D. dissertation, Massachusetts Insitute of Technology, 1997.

[18] Asakawa, "Two dimensional positioning device," US patent 4 626 749, Dec. 1986.

[19] H. S. Cho, C. H. Im, and H. K. Jung, "Magnetic field analysis of 2D permanent magnet array for planar motor," *IEEE Trans. Magn.*, vol. 37, no. 5, pp. 3762-3766, Sept.2001.

[20] J. Y. Cao, S. G. Wang, Y. Zhu, and W. S. Yin, "Modeling the static vertical force of the core-type permanent-magnet planar motor," *IEEE Trans. Magn.*, vol. 44, no. 12, pp. 4653-4658, Dec.2008.

[21] J. Y. Cao, S. G. Wang, Y. Zhu, and W. Xu, "Electromagnetic forces acting on the planar armature of a core-type synchronous permanent-magnet planar motor," *IEEE Trans. Magn.*, vol. 45, no. 8, pp. 3145-3150, Aug.2009.